Modelling the inflation of an elastic membrane with a load

Ge Shi[1], Azadeh Shariati[1], Jialei Shi[1], Nicolas Herzig[2], Sara-Adela Abad[1,3] and Helge A. Wurdemann[1]

Abstract— **One way to achieve large deformations and elongation in soft material robots involves the creation of structures made of a number of inflatable elastic membranes. Physical interactions between the inflated membranes or with their environment can lead to shape changes resulting in forces being exerted to the environment. In this paper, we present an analytical model to describe the inflation of a circular elastic membrane, which is constrained by a load, based on finite deformation theory. Our model will allow to understand the deformation, volume change and the height of the membrane. Our model can predict the height-pressure trend of the deformed membrane shape. Experimental validation includes the investigation of the membrane inflation under load, open-loop force control involving an inflated membrane, and the inflation of a stack of three actuators. The height-pressure model results lay within the experimental data and predicted the non-linear trend well. The model can be used for open-loop force control within a $\pm 15\%$ error. Also, we present the results for a manipulator made of a series of inflated membranes under load conditions.**

I. Introduction

Soft material robots offer a number of advantages including their flexibility, adaptability, and safe interaction, compared to traditional robots made of rigid materials [1]. The soft material that these robots are made of allow the systems to undergo large deformations, e.g., bending motions or elongation. Some soft actuators, such as the actuator presented by Connolly or the STIFF-FLOP actuator, can achieve elongations of around 100%, and 70%, respectively [2], [3]. In order to increase the level of deformation, some researchers have investigated to create soft manipulators made of thin membranes [4]. Inflating a structure composed of a series of thin membranes will the lead to a desired motion. For instance, Herzig *et al.* developed a highly extensible actuator joint based on the inflation of circular elastic membranes [5]. The hyperelastic balloon membranes demonstrate an overall extensibility of 179%. In addition, such a manipulator is capable of bearing weights of more than twenty times its own weight. Other soft actuators include the one proposed by Lee *et al.*. Here, a pneumatic 3-axis micro-actuator has been built based on balloons. The actuator was used as a haptic display to provide tactile information [6]. In fact, the inflation of a circular elastic membrane is also adopted to produce haptic stimuli in many applications [7]–[9]. One example has been proposed by Shi *et al.* adopting the inflation of a circular elastic membrane to produce haptic stimuli in prostheses. Their proposed system is purely mechanical driven, where the compression force is transmitted from an ellipsoid fingertip to the feedback actuator when the finger physically interacts with the environment [10].

Extensive research on the inflation of hyperelastic membranes has been explored. Treloar, for the first time, characterised the inflation of a rubber sheet [11]. The theory of non-linear membranes has been presented by Green and Adkins [12]. Adkins and Rivlin introduced the large deformation theory to calculate the deformation arising in the inflation of a flat circular membrane [13]. Yang and Feng simplified the problem of large axisymmetric deformations of non-linear elastic membranes [14]. In their approach, a set of second-order ordinary differential equations (ODE) were developed compared to the Adkin and Rivlin model, which was a large set of equations [13], [14]. Feng and Yang studied the mechanical and geometrical behaviour of an inflated spherical non-linear membrane compressed with two flat plates, considering the thermodynamic property of the compressible fluid that filled the membrane [15]. Feng and Huang analysed the behaviour of an inflated membrane undergoing compression with a rigid surface in which the contact was not axisymmetric [16].

Recent models include the inflation of different pre-shaped membranes such as sphere and torus, contact of the membrane with various contact shapes and different stiffness of the shapes [17]–[21]. For instance, Yang *et al.* analytically investigated the behaviour of inflat

ed circular membranes with large deformation in contact with various interfaces of the concave, convex, upper hemisphere and lower hemispheres. The analytical solution was validated with experimental results [21]. Bourmel *et al.* studied the membrane inflated and compressed with compressible fluid experimentally and numerically. The relationship between the change in shape and the applied force is explained by their analytical model [17].

Overall, interactions between a number of elastic membranes or membranes and their environment become interesting for the design and application of soft robotic manipulators. Of particular interest would be the relationship between their deformation, internal pressure and forces, that inflated elastic membranes are able to exert. Here, an analytical model based on finite deformation theory could be helpful to model the membrane inflation under load predicting the deformed shape of the membrane and inflation height.

This work is supported by the Engineering and Physical Sciences Research Council (grant numbers: EP/S014039/1, EP/V01062X/1), the Royal Society (RGS/R2/222228) and UCL Global Engagement.

[1]G. Shi, A. Shariati, J. Shi, S.-A. Abad, and H.A. Wurdemann are with the Department of Mechanical Engineering, University College London, UK. h.wurdemann@ucl.ac.uk

[2]Nicolas Herzig is with the School of Engineering and Informatics, University of Sussex, UK.

[3]S.-A. Abad is also with the Institute for Applied Sustainability Research, 170503, Quito, Ecuador.

The contribution of this paper lies in the presented analytical model describing the inflation of a circular elastic membrane, which is constrained by a load, based on finite deformation theory (see Fig. 1). Our model will allow us to understand the deformation, volume change and the height of the membrane. To validate our model, experimental results include the analysis of the inflation process of membranes with different dimensions under load. The experimentally validated model could benefit soft robotics and haptic systems made of membrane actuators, such as membrane inflation, the force controlling and the stack of actuators design.

This paper will be structured as follows: the introduction of the analytical model is presented in Section II. Section III introduces the experimental protocol, setup and results. The experiments contain validation, the control application of the model and the inflation of a stack of three actuators. Section IV discusses the results and compares the computational and experimental results. Conclusions are presented in Section. V.

II. Analytical Model of an Elastic Membrane

The assumption for the analytical model include:

- The circular elastic membrane is axisymmetric in the undeformed and deformed conditions. The shear stresses are zero from the profile view.
- The thickness of the ellipsoid membrane h_t is small relative to the radius (i.e., $(h_t)/(r_0) \ll 1$). Therefore, the change of thickness during deformation is considered negligible.
- The pressure under the contact region is evenly distributed and equal to the pressure inside the membrane.

The flat circular elastic membrane with a radius r_0 is inflated quasi-statically by a pressure p_0. The load M exerts force F_m on the membrane and vertically constrains the inflation to a height h_0 as shown in Fig. 1. In Fig. 1(a), a circular elastic membrane (in blue colour) with radius r_0 is constrained on its edge. A rigid flat load with a smooth surface is located on top of the membrane. In Fig. 1(b), by applying an air pressure p_0 into the membrane, the elastic membrane is inflated and the load is lifted vertically to the height h_0. The contact region between the load and the elastic membrane is flat, but the non-contact area of the membrane is able to inflate freely. The elastic membrane, in its undeformed status, is fitted into the cylindrical coordinates (x,θ,y) to describe the shape of the membrane. The origin of the coordinate frame is located in the centroid of the membrane. Cylindrical coordinates (ρ,θ,η) are used to mathematically describe the inflated membrane. As the membrane is axisymmetric along the η and y axes, the profile view of the undeformed membrane and inflated membrane is fitted into a Cartesian coordinate frame about (x,y) and (ρ,η). x_Γ denotes the value of x of the boundary between the contact and free inflation regions.

1) Potential energy function: The Mooney-Rivlin approach is applied to model the incompressible elastic material

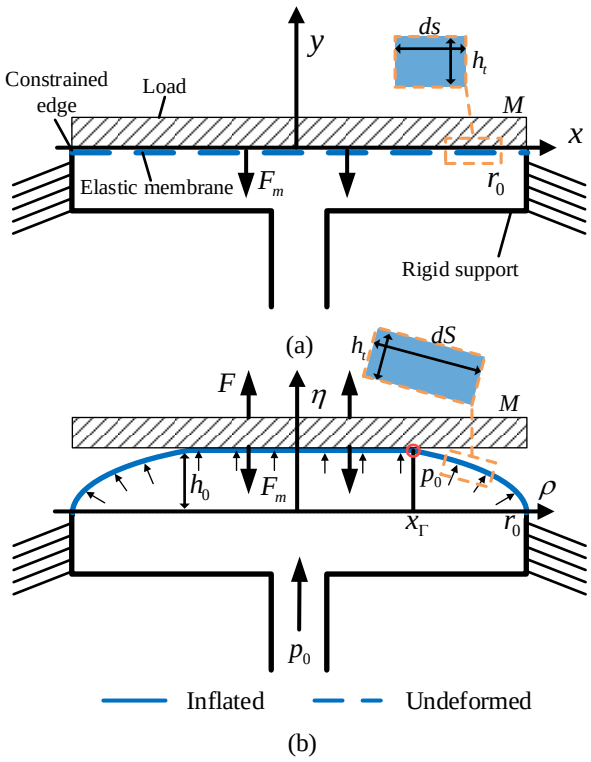

Fig. 1: Overview of an elastic membrane (blue line) being inflated and indented with a load in Cartesian coordinates. (a) The elastic membrane is fixed on the edge with a load M exerting a force on the top. (b) The elastic membrane is inflated with pressure p_0. The membrane inflates to height h_0, which is limited by the load. The enlarged view of the membrane shows the thickness of the membrane h_t and the infinitesimal arc length ds and dS of a segment.

of the membrane with the potential strain-energy function W, which is defined by (1).

$$W = C_1(I_1-3)+C_2(I_2-3), \tag{1}$$

with C_1 and C_2 defined as the material constants. The principal strain invariants I_1 and I_2 related to the principal stretch ratios, λ_1, λ_2, respectively, and defined as in (2).

$$\begin{aligned} I_1 &= \lambda_1^2+\lambda_2^2+\frac{1}{\lambda_1^2\lambda_2^2}, \\ I_2 &= \frac{1}{\lambda_1^2}+\frac{1}{\lambda_2^2}+\lambda_1^2\lambda_2^2. \end{aligned} \tag{2}$$

2) Free-inflation region: Along the axisymmetric elastic membranes, the infinitesimal arc length of the undeformed membrane is defined as ds lying on the horizontal axis x in the Cartesian coordinate frame as Fig. 1(a) shows. The inflated arc length is dS shown in Fig. 1(b) and defined in (3).

$$\begin{aligned} ds &= dx, \\ dS &= (d\rho^2+d\eta^2)^{1/2}. \end{aligned} \tag{3}$$

In this paper, variables with subscripts 1 and 2 represent the meridian and circumferential direction, respectively. The

primes in the equations are the derivatives of the horizontal position x.

The principal stretch ratios λ_1 and λ_2 are defined as the ratio between the undeformed lengths and the deformed lengths of an infinitesimal arc segment of the membrane. λ_1 and λ_2 are formulated in (4).

$$\begin{aligned} \lambda_1 &= \frac{dS}{ds} = (\rho\,'(x)^2 + \eta\,'(x)^2)^{1/2}, \\ \lambda_2 &= \frac{\rho(x)}{x}. \end{aligned} \tag{4}$$

The equilibrium equations for the free inflation region of the membrane in both meridian tangential and normal direction are described by (5).

$$\begin{aligned} \frac{dT_1}{d\rho} + \frac{1}{\rho}(T_1 - T_2) &= 0, \\ k_1 T_1 + k_2 T_2 &= p_0, \end{aligned} \tag{5}$$

where P is the pressure acting on the membrane. The stress resultants T_i of each membrane segment are given by (6).

$$T_i = 2h_t \frac{1}{\lambda_1 \lambda_2}\left(\lambda_i^2 \frac{\partial W}{\partial I_1} - \frac{1}{\lambda_i^2}\frac{\partial W}{\partial I_2}\right) \quad (i = 1,2). \tag{6}$$

By substituting (1) and (2), the T_1, T_2 are obtained in (7).

$$\begin{aligned} T_1 &= 2h_t C_1 \left(\frac{\lambda_1}{\lambda_2} - \frac{1}{\lambda_1^3 \lambda_2^3}\right)\left(1 + \frac{C_2}{C_1}\lambda_2^2\right), \\ T_2 &= 2h_t C_1 \left(\frac{\lambda_2}{\lambda_1} - \frac{1}{\lambda_1^3 \lambda_2^3}\right)\left(1 + \frac{C_2}{C_1}\lambda_1^2\right), \end{aligned} \tag{7}$$

where h_t is the membrane thickness. The principal curvature k_1 and k_2 is determined in (8).

$$\begin{aligned} k_1 &= \frac{(\rho'\eta'' - \eta'\rho'')}{(\rho'^2 + \eta'^2)^{3/2}}, \\ k_2 &= \frac{-\eta'}{\rho(\rho'^2 + \eta'^2)^{1/2}}. \end{aligned} \tag{8}$$

In the inflation region of the membrane, the variable ω is defined as $\omega = \frac{d\lambda_2 x}{dx}$. By substituting (4), (7) and (8) into (5), it is possible to obtain (9) as a function of $(\lambda_1, \lambda_2, \omega)$:

$$\begin{aligned} \lambda_1' &= \frac{\lambda_2 - \omega}{x}\frac{f_2}{f_1} + \frac{\omega}{\lambda_2 x}\frac{T_2 - T_1}{f_1}, \\ \lambda_2' &= \frac{\omega - \lambda_2}{x}, \\ \omega' &= -\frac{p_0 \lambda_1 (\lambda_1^2 - \omega^2)^{1/2}}{T_1} - \frac{\lambda_1^2 - \omega^2}{\lambda_2 x}\frac{T_2}{T_1} + \frac{\lambda_1'\omega}{\lambda_1}, \\ f_1 &= \frac{\partial T_1}{\partial \lambda_1}, f_2 = \frac{\partial T_1}{\partial \lambda_2}. \end{aligned} \tag{9}$$

The above set of equations applies to the inflation while $x_\Gamma < x < r_0$ (named as the inflated state). The height of the inflation membrane yields in (10).

$$h_0 = \widehat{\eta} = \int_{x_\Gamma}^{r_0} (\lambda_1^2 - \rho'^2))^{1/2} dx. \tag{10}$$

The volume within the membrane in the inflated state are described by (11).

$$V_{inf} = 2\pi \int_0^{\widehat{\eta}} \rho^2 d\eta. \tag{11}$$

3) Contact region: As shown in Fig. 1(b), the load with the rigid flat surface flattens the inflated membrane where in contact with the inflated membrane. The geometry of the flattened membrane within the contact region ($0 < x < x_\Gamma$) yields in (12).

$$\eta' = 0, (x < x_\Gamma). \tag{12}$$

Hence, the principal stretch in the contact region is in (13).

$$\begin{aligned} \lambda_1 &= \rho\,'(x), \\ \lambda_2 &= \frac{\rho(x)}{x}. \end{aligned} \tag{13}$$

Assuming no friction between the contact surfaces of the load and the membrane, the membrane is able to stretch freely during the inflation. The equilibrium states of the contact region are equivalent to the free inflation region. Substituting (7), (8) and (13) into (5), the system of equations $(\lambda_1, \lambda_2, \omega)$ governing in the contact region results in (14).

$$\begin{aligned} \lambda_1' &= -\frac{\omega - \lambda_2}{x}\frac{f_2}{f_1} - \frac{\omega}{\lambda_2 x}\frac{T_1 - T_2}{f_1}, \\ \lambda_2' &= \frac{\omega - \lambda_2}{x}, \\ \omega' &= \lambda_1', \\ f_1 &= \frac{\partial T_1}{\partial \lambda_1}, f_2 = \frac{\partial T_1}{\partial \lambda_2}. \end{aligned} \tag{14}$$

During the inflation, the force on the contact area acting on the load is calculated in (15).

$$F = A_c p_0 = \pi x_\Gamma^2 p_0, \tag{15}$$

where A_c is the contact area and p_0 the applied pressure in the inflated membrane.

4) Boundary conditions: The boundary conditions for the inflation with the load are formulated in (16).

$$\begin{aligned} x = 0 \quad & \lambda_1 = \lambda_2 = \lambda_0, \\ x = x_\Gamma \quad & \lambda_{1(contact\,region)} = \lambda_{1(inflation\,region)}, \\ x = x_\Gamma \quad & \lambda_{2(contact\,region)} = \lambda_{2(inflation\,region)}, \\ x = x_\Gamma \quad & \omega = \lambda_1', \\ x = r_0 \quad & \lambda_{2(inflation)} = 1. \end{aligned} \tag{16}$$

Hence, with a pressure p_0 and force F_m exerted on the membrane, the ideal contact area between the load and the membrane can be calculated as in (17).

$$A_c = \frac{F_m}{p_0}. \tag{17}$$

Due to the contact area being a circular shape, the radius of the contact area as well as the contact boundary x_Γ is given in (18).

$$x_\Gamma = \sqrt{\frac{F_m}{p_0 \pi}}. \tag{18}$$

5) Numerical solution procedure: The procedure of solving the set of ordinary differential equations describing the inflation of a circular elastic membrane with a load is present in Fig. 2. Firstly, the threshold of the minimum pressure p_min is calculated, where the load and the elastic membrane are in full contact with the entire surface of the membrane, i.e., this surface has the radius r_0, to lift the load with a height, which is calculated by (19).

$$p_{min} = \frac{F_m}{\pi r_0^2}. \tag{19}$$

After the pressure p_0 passes through the minimum pressure threshold, the membrane is inflated in the free inflation region. The contact boundary between the elastic membrane and the load is assumed as x_Γ. Given the initial condition $\lambda_1 = \lambda_2 = \lambda_0$ at $x = 0$, we apply the bisection method to find λ_0, so that the boundary conditions are satisfied, which is $\lambda_{2(inflation)} = 1$ at $x = r_0$. The force acting on the load is calculated by 15 and compared with the exerted force by the load to determine the equilibrium static states between the membrane and the load. If the force from the membrane is not equal to the force exerted by the load, the contact boundary x_Γ is re-assumed and then repeated the previous calculation until the results satisfy all the restrictions and conditions shown in (16)-(17). The ordinary differential equations are solved using the Runge Kutta method in Matlab 2022 with a tolerance of $10^{-2}\%$; the solution is usually obtained in less than 20 iterations.

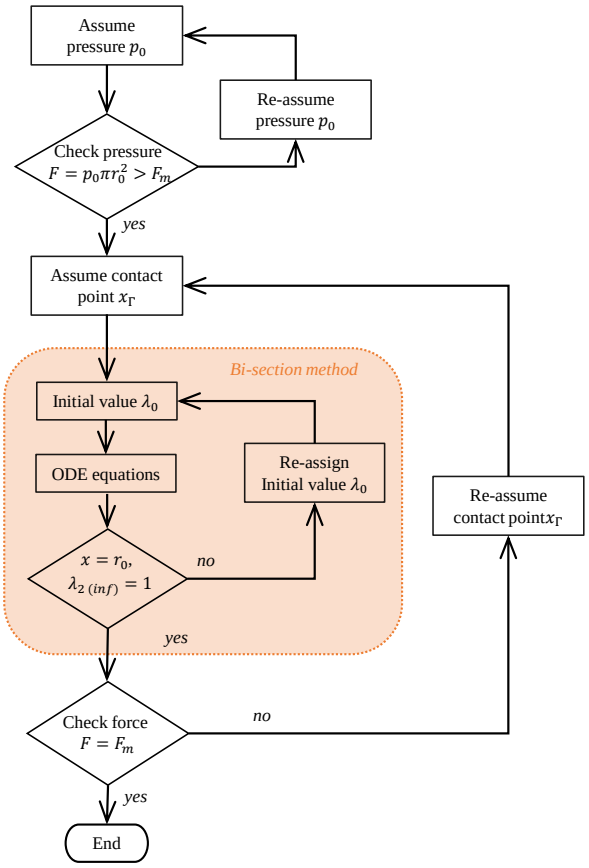

Fig. 2: Flow chart of calculations for solving the set of ordinary differential equations (9)-(14) for an elastic membrane inflation with a load.

III. Experiments: Validation and Application of the Analytical Model

A. Experiment 1: Validation of the analytical model

Protocol: Experiment 1 is designed to validate the analytical model, analysing the relationship between the height of the inflated membrane (called inflation height), applied pressure, and acting force on the load. The circular elastic membrane was fabricated with two radii of 10 mm and 15 mm and constrained on its edges to a test platform. Two loads of 50 g and 100 g were placed on the load bearing that is in full contact with the elastic membrane. The exerted force by the load is equal to the gravity of load itself in this configuration. By applying air pressure from 0 to 15 kPa to the membrane, the height of the inflated membrane was measured by an Aurora electromagnetic sensor. Each inflation trial was repeated for five times, and the average of the trials was reported.

Experimental setup: The test platform for Experiment 1 is shown in Fig. 3(a). The circular elastic membrane is made from Ecoflex 00-50 (Smooth-on, Inc.) with the thickness of $h_t = 2$ mm. It was constrained on a 3D printed platform (Formlab 3B, Though 2000). The hyperelastic property of Ecoflex 00-50 is determined by the strain-stress curve from a uniaxial tensile test, where the constants of the Mooney-Rivlin model are $C_1 = 8045$ Pa and $C_2 = 5015$ Pa. An air inlet located underneath ensures the inflation and deflation process. A rigid plate with a load is placed on top of the membrane. Two rods constrain the plate motion only in the vertical direction. An electromagnetic position sensor (NDI Aurora) is attached to the load tracking the inflation height. The pressure applied on the elastic membrane is controlled by a proportional pressure regulator (Camozzi K8P) to regulate and monitor the pressure. Pressurised air is supplied by a compressor (HYUNDAI Model HY5508).

Results: Fig. 3(b) shows the model results of the deformation of the 15 mm-radius membrane bearing a constant load of 100 g with the internal air pressure ranging from 2 kPa to 10 kPa. As the pressure increases, the height increases non-linearly, decreasing the contact boundary x_Γ marked by red dots in Fig. 3(b). The stiffness of the membrane increases with increasing inflation and pressure as well. The boundary of the membrane converges at 15 mm in line with the clamped membrane during the experiments.

The experimental results in Fig. 3(c) illustrate the relationship between the pressure p_0 and inflation height h_0 for two radii of (10 mm and 15 mm) under two loads (100 g and 200 g), respectively. The solid and dashed lines represent the results from the analytical model. The blue scatter represents the experimental results of the 15 mm membrane and the red scatters the results of the 10 mm membrane during inflation. Overall, the curves show a non-linear behaviour. For the 100 g load, the threshold of

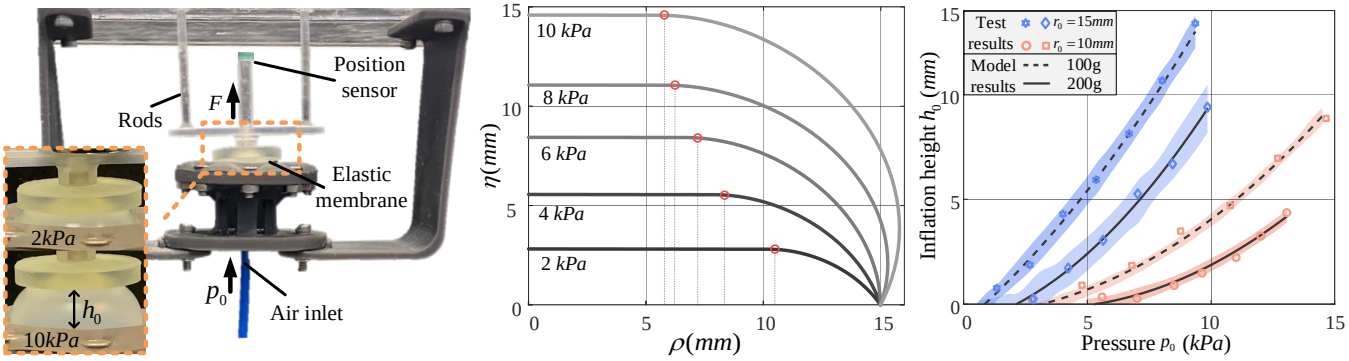

(a) (b) (c)

Fig. 3: (a) Setup for the validation of the inflation of a circular elastic membrane with a load (Experiment 1). The elastic membrane is clamped to its rigid parts with an air inlet being inserted from the bottom. A Aurora position sensor is mounted to the rods tracking the inflation height. The enlarged view shows the membrane deformation when inflated by 2 kPa and 10 kPa with a load of 100 g. (b) Deformation results from the analytical model of the 15 mm radius membrane calculated using 10. The membrane was inflated by a range of 2 kPa to 10 kPa with a 100 g load constraining the inflation process. The red points represent the contact boundary x_Γ. (c) Inflation height against pressure values from experimental and model results of two membranes ($r_0 = 10$ mm and $r_0 = 15$ mm) with 100 g and 200 g loads acting on the membrane.

minimum pressure p_{min} to achieve membrane inflation is 2.98 kPa for the 10 mm membrane and 1.41 kPa for the 15 mm membrane. For the 200 g load, p_{min} is 5.34 kPa and 2.56 kPa for the 10 mm and 15 mm membranes, respectively. As shown in Fig. 3, the non-linearity between the pressure and inflation height increases when the load increases or the radius decreases. Overall, the model results lay in with the experiment results and validated the analytical model.

B. *Experiment 2: Open-loop force control.*

Protocol: After the validation in Experiment 1, the application of our model as a control method is the focus of Experiment 2. Fig. 4(a) shows the open-loop diagram of the control system. The desired h_0 is sent to the linear rail driving the contact plate to a desired position, where the distance between the contact plate and the base of the membrane is h_0. The desired force F_m and desired h_0 are inputs to the controller. The controller computes the predicted pressure p_0 and sends the corresponding pressure values to the regulator controlling the pressure p_0 at the desired level. Then, the force F exerted to the contact plate to the inflated membrane is recorded by a sensor.

The elastic membrane with a 15 mm radius was selected in Experiment 2. The inflated membrane was in contact with the rigid contact plate, as shown in Fig. 4(b). The contact plate, which is attached to a force sensor, is moved in a range between $h_0 = 5$ mm to 15 mm. Two force values were chosen to be maintained by the rigid plate, which are $F_m = 1$ N and 2 N. The results are reported in Fig. 5.

Experimental setup: A workbench was built for Experiment 2, which contains a linear rail (Zaber X LSM100A) and a 6-axis force sensor (IIT FT17). The elastic membrane was clamped on a 3D-printed platform with an air inlet inserted at the bottom. The pressure was controlled by a proportional pressure regulator (Camozzi K8P) with an air compressor (HYUNDAI Model HY5508) providing pneumatic pressure.

Results: Fig. 5 shows the experimental and analytical results for five trials running for 120 seconds. Each trial

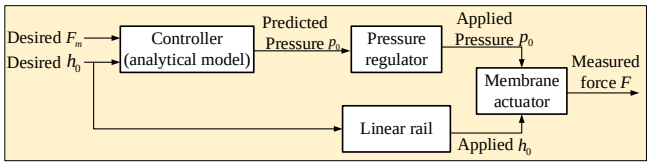

(a)

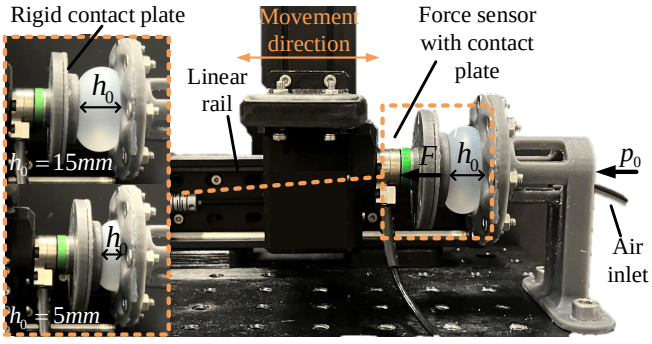

(b)

Fig. 4: (a) Open-loop control diagram for the implementation of our analytical model. (b) Setup for Experiment 2. The elastic membrane is fixed on the workbench with an air inlet at the bottom. A FT-17Force sensor with the contact plate opposing the membrane is mounted to a linear rail. The force sensor can sense the force that the pressurised membrane exerts to the rigid plate. The enlarged views show the inflated elastic membranes with the force sensor and contact plate when the measured distances h_0 are 5 mm and 15 mm.

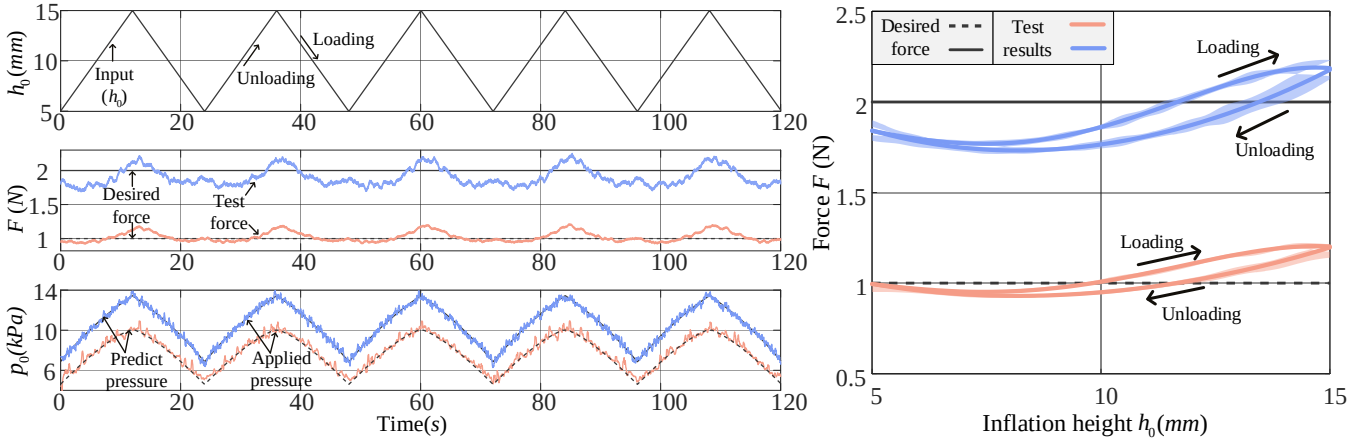

Fig. 5: Experimental and computational results for the open-loop control of the membrane inflation with a 15 mm radius and 2 mm thickness (Experiment 2). (a) Results of five trials running 120 seconds. As the movement of the contact plate with the force sensor changes in the distance h_0 from 5 mm to 15 mm, the predicted pressure p_0 regarding the h_0 was applied on the membrane resulting in the force F measured by the force sensor to maintain at a constant force value (1 N to 2 N). (b) Non-linear force on the contact plate versus displacement of five trails.

contains two stages: the unloading (contact plate moving away from the membrane from 5 mm to 15 mm) and loading stage (contact plate approaching the membrane from 15 mm to 5 mm). According to the measured distance h_0, the pressure p_0 was calculated based on the interpolation results from the model. This values is then applied to the membrane in the experiment resulting in the force acting on the contact plate. The non-linear behaviour of increasing and decreasing the pressure p_0 is synchronised with the change of displacement h_0. During the test, the fluctuation of the applied pressure results in an unstable force output. The pressure fluctuation is similar for the 1 N and 2 N trials. However, it can be observed that the fluctuation is slightly more intensive for the 2 N trial. This might be due to the sensitivity of the membrane increasing when a larger load of pressure level is applied to the membrane.

The relationship between the membrane displacement versus the acting force is shown in Fig. 5(b) for five repetitions. The acting force for the 1 N and 2 N trial is within $\pm 15\%$ error. In Fig. 5(b), the maximum error for the 1 N trial is at around 15 mm displacement, exceeding an average of 14.3% for the 1 N trial. For the 2 N condition, the maximum error points are at 7.5 mm displacement, equivalent to a relative average error of 12.2%. In addition, the hysteresis has a value of 12.84% at 12.4 mm displacement and 22.47% at 13.1 mm displacement corresponding for the 1 N condition and 2 N condition, respectively.

C. Experiment 3: Application of the analytical model with a stack of actuators

Protocol: To investigate the application of our analytical model to the application of soft robotic systems made of inflatable membranes such as presented in [5], a stack of three actuators, driven by the inflation of circular elastic membranes, was built. All actuators have a 15 mm radius membrane and were placed vertically on top of each other. Applying the same pressure ranging from 0 kPa to 15 kPa, the total inflation height (Δh) for a 200 g load was measured and is compared with the results of the analytical model calculating the total inflation height ($\Delta h = h_{01} + h_{02} + h_{03}$).

Experimental setup: Fig. 6(a) presents the experimental setup for the stack test. Three actuators are stacked vertically with three rods constraining the one-directional movement. The circular elastic membranes, which are made of Ecoflex 50-00, have a 15 mm radius and 2 mm thickness. The actuators were mounted on a 3D-printed rigid case to ensure a one-directional movement. An electromagnetic position sensor (NDI Aurora) was attached to the load to track the inflated height of the load. The pressure of each actuator was controlled by a proportional pressure regulator (Camozzi K8P), and an air compressor (HYUNDAI Model HY5508) provided the pneumatic power.

Results: Fig. 6(b) shows the results of the inflation height h_0 of a single membrane, which is calculated by the analytical model with varied load (force) from 0 N to 4 N and pressure p_0 from 0 kPa to 15 kPa. The interpolation of the calculated results shows a non-linear surface. As the pressure increases, the inflation height increases in a non-linear way. The increase of the membrane load or acting force results in the non-linear decrease of the height as well. With the regressed model, the inflation height can be calculated with pressure and force as inputs.

In order to calculate the inflation of the stack, loads for each actuator were calculated. The measured weight of the actuator and rigid case is 20 g. Hence, the load of the top actuator is 200 g, 220 g for the middle and 240 g for the

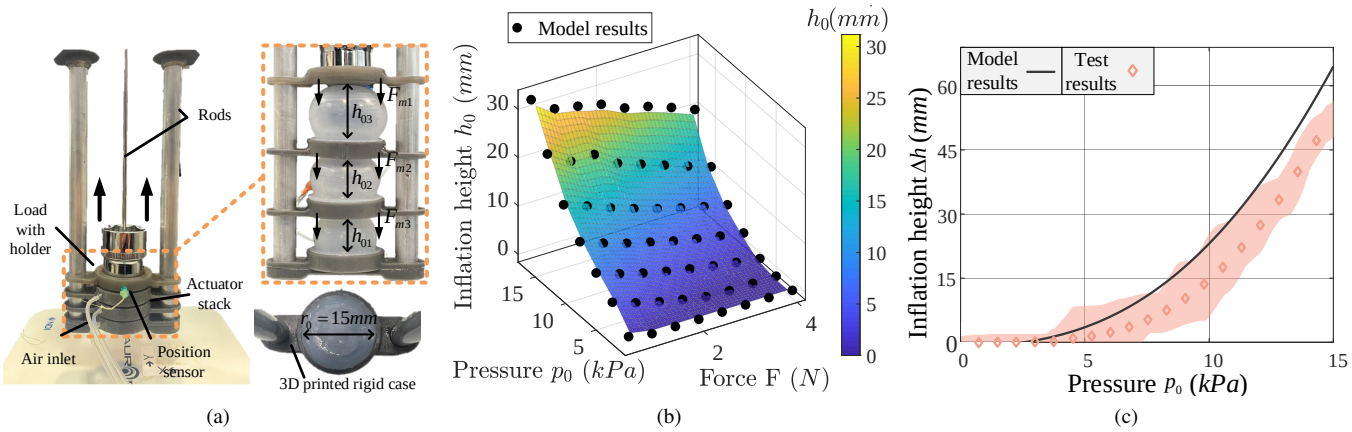

(a) (b) (c)

Fig. 6: (a) Three actuators with a 15 mm radius membrane are stacked vertically. A load is placed at the top. Rods ensure the stack movement in vertical direction only. The enlarged view shows the stack when actuated by 15 kPa pressure. (b) The interpolation results from the analytical model with inflation height h_0, pressure p_0 and acting force F. (c) Inflation height Δh against applied pressure p_0 for the experimental and model results for the stack of three actuators being inflated by pressure values between 0 kPa to 15 kPa.

bottom actuator, respectively. Fig. 6(c) shows the relationship of the inflation height versus the pressure applied to three actuators of five trials. The threshold for the minimum pressure p_{min} of inflation is 3.23 kPa for the top actuator. The bottom two actuators remain undeformed here. As the pressure increases, the inflation height of the load increases non-linearly, reaching 51.23 mm inflation height. For the pressure range of 0 kPa to 10 kPa, the experimental and model results show an agreement with trend of the non-linear behaviour. As the pressure increases further, the deviation between the model results and the experimental increases.

IV. Discussions

Looking at the results for Experiment 1, the model shows an agreement with the experimental results. As the load of the membrane increases, the non-linearity of the inflation height versus the applied pressure becomes notable. Especially at the beginning of the inflation, the membrane is relatively soft and able to resist the load. As the pressure increases, the inflated membrane becomes stiffer, and the effect of the load compression is less significant, which results in the rapid height increase when the pressure is increased. Due to the fact that the membrane material is hyperelastic, the membrane expands in a non-linear way with increasing pressure values as shown in Fig. 3(b).

Experiment 2 then demonstrates the versatility of the analytical model. In order to control the membrane inflation in real time, an regressed relationship between the inflation height and pressure was applied. The results show the model can predict the force acting on the object by the membrane inflation for the 1 N and 2 N trial with the error being below 14.3% and 12.2%, respectively. However, the hysteresis increases with larger loading and pressure level since the non-linear elasticity of the membrane becomes notable as the pressure increases.

For Experiment 3, a three dimensional interpolation in Fig. 6(b) was applied to calculate the inflation of the stack of actuators. The rate of the non-linearity of the inflation height and pressure (Fig. 6(c)) are similar for the model and experimental results. It can be observed that the deviation proportionally increases as the pressure increases. Manifold reasons might be the cause for this discrepancy. Firstly, friction exists in many kinetic contacts, such as the contact between elastic membranes and rigid components and actuators with rods. Despite the contacts being lubricated by synthetic oil, the friction between actuators becomes significant at a high loading level. The increase of friction results in less membrane releasing the contact and being able to inflate freely. In addition, the adhesive contact between the membrane and rigid case might strengthen in varied conditions.

As mentioned in the beginning of the paper, a number of assumptions for the analytical model have been made. Firstly, a potential change in the membrane's thickness was not considered during the calculation since the thickness of the membrane is significantly smaller than the radius r_0 of the membrane. Hence, one limitation might occur if the membrane thickness would be increased. In addition, the assumption of the smooth contact between the elastic membrane and the load surface is notable. In this paper, the contacts between the elastic membrane and load in every experiment were lubricated by synthetic oil and reduced the friction and adhesive contact significantly. The lack of lubrication might cause a deviation between the experimental and model results.

V. Conclusion

This paper presents and validates an analytical model based on the finite deformation theory to model the inflation

of a circular elastic membrane with a constant load, as well as validates the model based on the experimental results. This model is capable of calculating the non-linear increase of the inflation height against pressure, and the results are in line with the experimental data(Fig. 3(c)). In our approach, the boundary conditions of the ODEs are varied to adapt to different cases. By setting up the dimension of the membrane(r_0, h_t), material property(C_1, C_2), desired force(F) and pressure(p_0), the inflation can be solved with the results of inflation height(h_0) and deformed shape as illustrated in Fig. 3(b) and (c). In experiment 2, the interpolation of the model results can be applied to a control strategy to maintain a constant force level on a moving object. In experiment 3, a stack of three actuators, which are actuated by the inflation of the circular elastic membrane, was built, and the model can predict the trend of the stack inflation.

Our analytical model can predict the inflated membrane with a constant load. Hence, by designing the membrane actuators for soft robotics and haptic systems with different dimensions with different materials, the model can predict the deformation of the membrane at varying loading levels and optimise the design to replicate the height-pressure curve. The deformation theory for the elastic membrane is not limited to the soft robotic and haptic systems and has the potential ability to model in manifold cases.

In the future, we aim to simplify the complexity of the ODEs and calculation algorithm, which is capable of real-time control cases with deformed membrane output. Furthermore, rather than vertical inflation, contact between the membrane and the object at different angle need to be investigated. And the fiction in the contact needs to be considered to increase the model's accuracy.

REFERENCES

[1] P. Polygerinos, N. Correll, S. A. Morin, B. Mosadegh, C. D. Onal, K. Petersen, M. Cianchetti, M. T. Tolley, and R. F. Shepherd, "Soft robotics: Review of fluid-driven intrinsically soft devices; manufacturing, sensing, control, and applications in human-robot interaction," *Advanced Engineering Materials*, vol. 19, no. 12, p. 1700016, 2017.

[2] F. Connolly, C. J. Walsh, and K. Bertoldi, "Automatic design of fiber-reinforced soft actuators for trajectory matching," *Proceedings of the National Academy of Sciences*, vol. 114, no. 1, pp. 51–56, 2017.

[3] J. Shi, W. Gaozhang, and H. A. Wurdemann, "Design and characterisation of cross-sectional geometries for soft robotic manipulators with fibre-reinforced chambers," in *IEEE 5th International Conference on Soft Robotics (RoboSoft)*. IEEE, 2022, pp. 125–131.

[4] C. Laschi, B. Mazzolai, and M. Cianchetti, "Soft robotics: Technologies and systems pushing the boundaries of robot abilities," *Science Robotics*, vol. 1, no. 1, p. eaah3690, 2016.

[5] N. Herzig, J. Jones, E. Perez-Guagnelli, and D. D. Damian, "Model and validation of a highly extensible and tough actuator based on a ballooning membrane," in *IEEE International Conference on Robotics and Automation (ICRA)*. IEEE, 2021, pp. 11 961–11 967.

[6] E.-H. Lee, S.-H. Kim, and K.-S. Yun, "Three-axis pneumatic haptic display for the mechanical and thermal stimulation of a human finger pad," in *Actuators*, vol. 10, no. 3. MDPI, 2021, p. 60.

[7] J. J. Huaroto, E. Suarez, H. I. Krebs, P. D. Marasco, and E. A. Vela, "A soft pneumatic actuator as a haptic wearable device for upper limb amputees: Toward a soft robotic liner," *IEEE Robotics and Automation Letters*, vol. 4, no. 1, pp. 17–24, 2018.

[8] R. E. Fan, M. O. Culjat, C.-H. King, M. L. Franco, R. Boryk, J. W. Bisley, E. Dutson, and W. S. Grundfest, "A haptic feedback system for lower-limb prostheses," *IEEE Transactions on Neural Systems and Rehabilitation Engineering*, vol. 16, no. 3, pp. 270–277, 2008.

[9] C. Antfolk, A. Björkman, S.-O. Frank, F. Sebelius, G. Lundborg, and B. Rosen, "Sensory feedback from a prosthetic hand based on air-mediated pressure from the hand to the forearm skin," *Journal of Rehabilitation Medicine*, vol. 44, no. 8, pp. 702–707, 2012.

[10] G. Shi, A. Palombi, Z. Lim, A. Astolfi, A. Burani, S. Campagnini, F. G. Loizzo, M. L. Preti, A. M. Vargas, E. Peperoni *et al.*, "Fluidic haptic interface for mechano-tactile feedback," *IEEE Transactions on Haptics*, vol. 13, no. 1, pp. 204–210, 2020.

[11] L. Treloar, "Strains in an inflated rubber sheet, and the mechanism of bursting," *Rubber Chemistry and Technology*, vol. 17, no. 4, pp. 957–967, 1944.

[12] A. Green, "Large elastic deformations," 1960.

[13] J. E. Adkins and R. S. Rivlin, "Large elastic deformations of isotropic materials ix. the deformation of thin shells," *Philosophical Transactions of the Royal Society of London. Series A, Mathematical and Physical Sciences*, vol. 244, no. 888, pp. 505–531, 1952.

[14] W. H. Yang and W. W. Feng, "On Axisymmetrical Deformations of Nonlinear Membranes," *Journal of Applied Mechanics*, vol. 37, no. 4, pp. 1002–1011, 12 1970.

[15] W. W. Feng and W.-H. Yang, "On the Contact Problem of an Inflated Spherical Nonlinear Membrane," *Journal of Applied Mechanics*, vol. 40, no. 1, pp. 209–214, 03 1973.

[16] W. W. Feng and H. Pangnan, "On the general contact problem of an inflated nonlinear plane membrane," *International Journal of Solids and Structures*, vol. 11, no. 4, pp. 437–448, 1975.

[17] Y. Bouremel, I. Eames, S. Madaan, S. Brocchini, and P. T. Khaw, "Compression of pressurised elastic pockets," *International Journal of Non-Linear Mechanics*, vol. 107, pp. 10–15, 2018.

[18] X. Li and D. Steigmann, "Finite deformation of a pressurized toroidal membrane," *International Journal of Non-linear Mechanics*, vol. 30, no. 4, pp. 583–595, 1995.

[19] N. Kumar and A. DasGupta, "On the contact problem of an inflated spherical hyperelastic membrane," *International Journal of Non-Linear Mechanics*, vol. 57, pp. 130–139, 2013.

[20] A. Patil, A. DasGupta, and A. Eriksson, "Contact mechanics of a circular membrane inflated against a deformable substrate," *International Journal of Solids and Structures*, vol. 67, pp. 250–262, 2015.

[21] X. Yang, L. Yu, and R. Long, "Contact mechanics of inflated circular membrane under large deformation: Analytical solutions," *International Journal of Solids and Structures*, vol. 233, p. 111222, 2021.